Measurement of the ^{169}Tm$(n, 3n)^{167}$Tm cross section and the associated branching ratios in the decay of ^{167}Tm

B. Champine,[1,2] M. E. Gooden,[3] Krishichayan,[4,5] E. B. Norman,[1,2,6] N. D. Scielzo,[2] M. A. Stoyer,[2] K. J. Thomas,[1,6] A. P. Tonchev,[2] W. Tornow,[4,5] and B. S. Wang[1]

[1]*Department of Nuclear Engineering, University of California, Berkeley, California 94720, USA*
[2]*Nuclear and Chemical Sciences Division, Lawrence Livermore National Laboratory, Livermore, California 94551 USA*
[3]*Nuclear and Radiochemical Group, Los Alamos National Laboratory, Los Alamos, New Mexico 87545, USA*
[4]*Department of Physics, Duke University, Durham, North Carolina 27708, USA*
[5]*Triangle Universities Nuclear Laboratory, Durham, North Carolina 27708, USA*
[6]*Nuclear Science Division, Lawrence Berkeley National Laboratory, Berkeley, California 94720 USA*

(Received 4 November 2015; published 14 January 2016)

The cross section for the ^{169}Tm$(n,3n)^{167}$Tm reaction was measured from 17 to 22 MeV using quasimonoenergetic neutrons produced by the ^{2}H$(d,n)^{3}$He reaction. This energy range was studied to resolve the discrepancy between previous $(n,3n)$ cross-section measurements. In addition, the absolute γ-ray branching ratios following the electron-capture decay of ^{167}Tm were measured. These results provide more reliable nuclear data for an important diagnostic that is used at the National Ignition Facility to estimate the yield of reaction-in-flight neutrons produced via the inertial-confinement-fusion plasma in deuterium-tritium capsules.

DOI: 10.1103/PhysRevC.93.014611

I. INTRODUCTION

The National Ignition Facility (NIF) at Lawrence Livermore National Laboratory is designed to drive deuterium-tritium (DT) inertial-confinement-fusion targets to ignition. As a result of DT fusion, neutrons are produced via the ^{3}H$(d,n)^{4}$He reaction with energies $E_n = 14.1$ MeV. Higher-energy neutrons can be created when a D or T ion brings kinetic energy gained from elastic scattering with a fusion product in the plasma to the DT reaction. This multistep process produces so-called reaction-in-flight (RIF) neutrons with energies up to 30 MeV. Although the RIF neutrons represent less than 0.3% of the total neutron fluence, their spectrum carries important information about the fusion burn and charged-particle stopping powers in a warm, dense plasma [1–3].

A representative NIF neutron-energy spectrum [3] from DT fusion is shown in Fig. 1. The 15-MeV threshold for the ^{169}Tm$(n,3n)^{167}$Tm reaction makes thulium a useful diagnostic for measurement of the RIF neutrons in the presence of copious 14-MeV neutrons. ^{167}Tm also has convenient production and decay characteristics: a large $(n,3n)$ cross section, a convenient half-life ($t_{1/2} = 9.2$ days), and an intense γ-ray transition (with energy $E_\gamma = 207.8$ keV and γ-ray emission branching ratio $I_\gamma = (42 \pm 8)\%$). Because ^{168}Tm is also produced from stable ^{169}Tm through the $(n,2n)$ reaction by 14.1-MeV neutrons, the ratio of ^{167}Tm to ^{168}Tm produced in a thulium monitor foil can provide a measure of the RIF neutron yield. The activation of foils at NIF and the subsequent offline counting using a Compton-suppressed high-purity germanium (HPGe) clover system to suppress backgrounds from the decay of ^{168}Tm was successfully used to measure ^{167}Tm production and therefore determine the yield of RIF neutrons [3].

In Fig. 2, the previously published ^{169}Tm$(n,3n)$ cross-section measurements are shown [4–6]. In Ref. [5], the ^{169}Tm$(n,3n)$ reaction was measured using a large tank of gadolinium-loaded liquid scintillator to detect the emitted neutrons. In Ref. [6], the reaction was determined by using a NaI(Tl) well detector, while the neutron fluence was determined by proton-recoil telescope measurements. As can be seen, the experimental data for the ^{169}Tm$(n,3n)$ cross section is discrepant at energies above 19 MeV. Because the production of ^{167}Tm depends on both the RIF neutron-energy spectrum, which is dropping off above 15 MeV, and the ^{169}Tm$(n,3n)$ cross section, which is increasing from 15–25 MeV, the largest contribution to ^{167}Tm production from a typical NIF shot is from the neutrons near 20 MeV in energy. Therefore, the 15%–20% disagreement between the previous $(n,3n)$ cross-section results in this energy region is concerning.

The easiest way to identify the presence of ^{167}Tm in an activation foil is by detection of the 207.8-keV γ ray emitted following the electron-capture (EC) decay of the nucleus. However, to quantify the yield of ^{167}Tm, the branching ratio of this γ ray must be accurately known. A current limitation is that this branching ratio, although large, had previously only been measured with a fractional precision of 19% [7]. The other γ rays emitted in the decay, such as the 531.5-keV γ ray with $I_\gamma = (1.61 \pm 0.22)\%$, have significantly smaller branching ratios which make it difficult to collect sufficient statistics to identify a peak especially with the large background from ^{168}Tm in an activated sample.

In this work, two independent experiments were conducted to improve the nuclear data for the ^{169}Tm$(n,3n)^{167}$Tm reaction cross section and the branching ratio of the 207.8-keV γ ray to allow a better determination of the number of RIF neutrons, which in turn provides valuable information for understanding the burn characteristics of an NIF plasma. The branching ratio for the 207.8-keV γ ray following ^{167}Tm EC decay was measured precisely using facilities at Lawrence Berkeley National Laboratory (LBNL) and the University of California at Berkeley. With this improved branching ratio, a subsequent experiment was conducted to measure the ^{169}Tm$(n,3n)^{167}$Tm cross section using the 10-MV Van

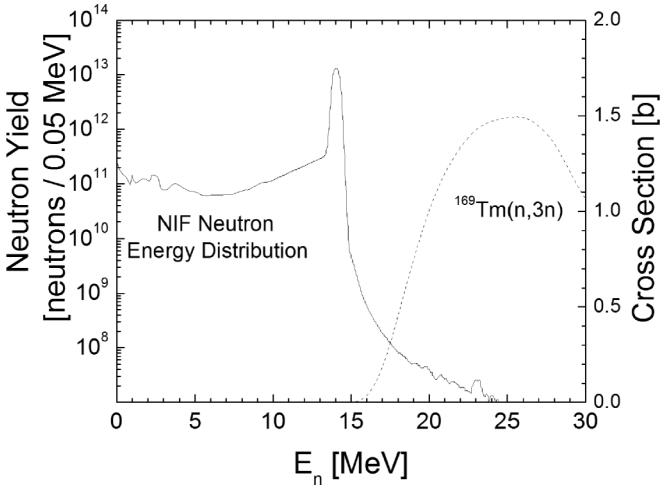

FIG. 1. Overlay of a simulated NIF neutron-energy distribution (y axis on left side) and the ^{169}Tm$(n,3n)$ ^{167}Tm cross section (y axis on right side). Only reaction-in-flight neutrons have enough energy to produce ^{167}Tm.

de Graaff accelerator at the Triangle Universities Nuclear Laboratory (TUNL).

II. ^{167}Tm BRANCHING-RATIO MEASUREMENT

A. Experiment

A 32-μm-thick ^{165}Ho foil was irradiated using an α-particle beam at the 88-Inch Cyclotron at LBNL to induce the ^{165}Ho$(\alpha,2n)$ ^{167}Tm reaction. In addition to ^{167}Tm ($t_{1/2}$ = 9.25 d), ^{168}Tm ($t_{1/2}$ = 93.1 d), and ^{166}Tm ($t_{1/2}$ = 7.70 h) isotopes were produced by the ^{165}Ho(α,n) and ^{165}Ho$(\alpha,3n)$ reactions, respectively. With its shorter half-life, ^{166}Tm could be allowed to decay to stable ^{166}Er prior to measurement. An α-beam energy of 29 MeV was selected so that the induced activity of ^{168}Tm was initially less than 0.5% of that of the desired

TABLE I. Activation samples for branching-ratio and cross-section measurements.

Target	Purity (%)	Thickness (μm)
^{165}Ho[a]	99.9	32(3)
^{169}Tm[a]	99.9	261(4)
^{nat}Ni	99.994	514(8)
^{nat}Zr (2.02% Hf)	97.91	241(4)

[a]Monoisotopic.

^{167}Tm. Foil thickness was determined from the area and mass, and verified with calipers and γ-ray attenuation measurements. The ^{165}Ho foil properties are summarized in Table I.

The x rays and γ rays from the activated foil were counted using both coaxial and planar HPGe detectors. Efficiencies for each detector were determined using ^{57}Co, ^{133}Ba, ^{137}Cs, ^{152}Eu, and ^{241}Am calibration sources. The calibration and foil counting was performed at a distance of 25 cm to minimize geometry uncertainties and avoid true-coincidence summing. The finer resolution and flatter efficiency curve of the planar HPGe detector in the lower-energy region was preferable for measuring the x rays. A sample spectrum measured with the planar HPGe detector is shown in Fig. 3. Self-attenuation of the emitted x rays and γ rays in the foil was calculated using the foil thickness and photon cross sections [8,9]. These corrections were less than 6% for the x rays, and were much smaller for the higher-energy γ rays.

B. Results

The 49.128-keV $K_{\alpha 1}$ x ray emitted from ^{167}Er following ^{167}Tm EC was used to determine the activity of ^{167}Tm in the sample. The γ-ray branching ratios, I_γ, were then determined from

$$I_\gamma = \frac{\epsilon_x a_x}{\epsilon_\gamma a_\gamma} \frac{N_\gamma P_{K_{\alpha 1}}}{N_x}, \quad (1)$$

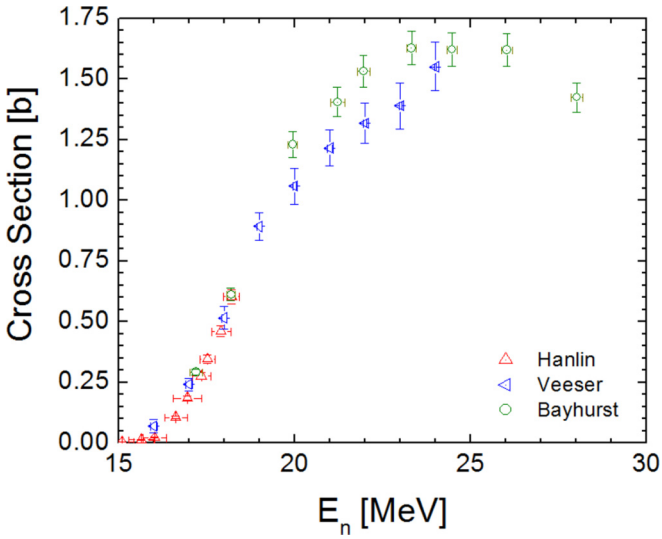

FIG. 2. ^{169}Tm$(n,3n)$ cross-section data [4–6] from the EXFOR database.

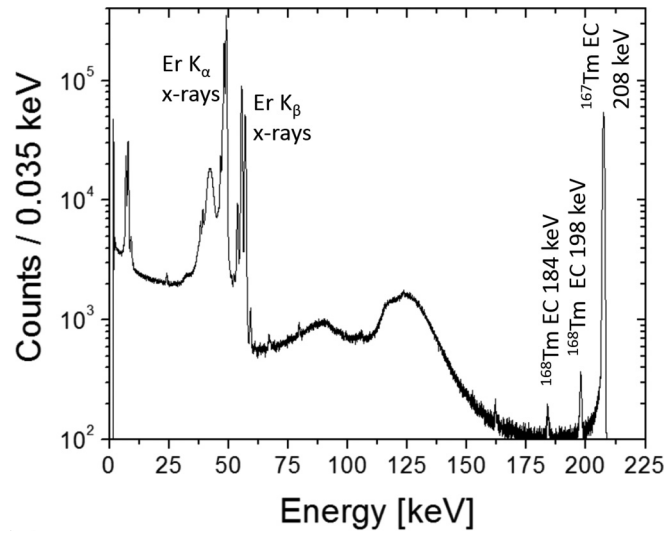

FIG. 3. Energy spectrum of the irradiated holmium foil measured using a planar HPGe detector.

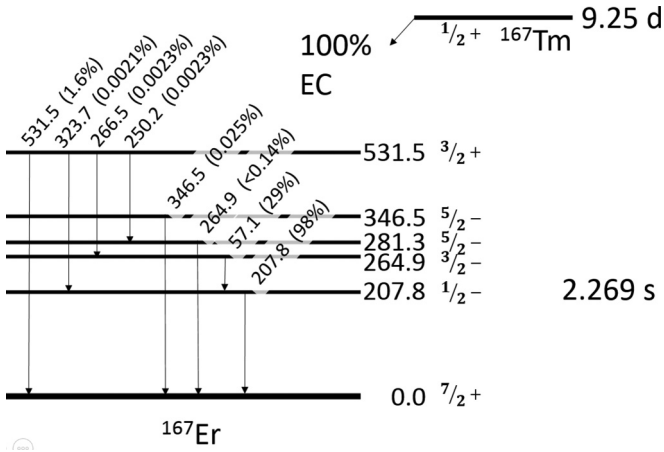

FIG. 4. Relevant decay scheme properties for the electron-capture decay of ^{167}Tm. All energies are given in keV [10].

where ϵ is the photopeak efficiency, a is the self-attenuation factor, and N is the number of counts in the peak of interest for the measured x rays and γ rays denoted by the subscripts x and γ, respectively, after correcting for x-ray contributions from the decay of ^{168}Tm as described below. $P_{K_{\alpha 1}}$ is the probability of $K_{\alpha 1}$ x-ray emission following the EC decay. The K_β x rays were not used here because of the interference with the 57.1-keV γ ray following ^{167}Tm decay.

The value of $P_{K_{\alpha 1}}$ was calculated from the product of the total number of K-shell vacancies per decay and the probability of that vacancy resulting in the emission of a $K_{\alpha 1}$ x ray. The K-shell vacancies may be caused by the EC transition as well as any subsequent internally converted transitions as ^{167}Er de-excites to the ground state. The number of K-shell vacancies per decay from the EC transitions was calculated to be 0.8096(13) using values from Ref. [11] and the existing decay scheme [10], summarized in Fig. 4. The additional K-shell vacancies from emission of internal conversion electrons from the excited daughter nucleus, primarily from the $E3$ transition of the first excited state at 207.8 keV, was calculated to be 0.1970(34) per decay using the BrIcc database for theoretical internal conversion coefficients [12]. This probability of creating a K-shell vacancy was then multiplied by the probability of $K_{\alpha 1}$ x-ray emission, which is 47.5(10) per 100 K-shell vacancies from Table 7A of Ref. [13]. A value of $P_{K_{\alpha 1}} = 0.478(10)$ was obtained, with an uncertainty dominated by the uncertainty in the $K_{\alpha 1}$ x-ray intensity per K-shell vacancy.

The correction for the number of x rays emitted from the EC decay of the longer-lived ^{168}Tm was calculated in a similar manner, with the activity determined from the measured 184-keV and 198-keV γ-ray peaks associated with this decay, as the γ-ray branching ratios are precisely known. This correction was only 0.4% (with negligible uncertainty) because of the small amount of ^{168}Tm activity in the sample.

The results and uncertainties are summarized in Table II. The 207.8-keV and 531.5-keV γ-ray branching ratios were measured to be 0.419(16) and 0.0173(7), respectively. The branching ratios were determined with a relative uncertainty of about 3.8%, which is a factor of five better than the previous measurement [10].

TABLE II. Branching-ratio results for ^{167}Tm. The measured branching ratios for the 207.8-keV and 531.5-keV γ rays are provided in the last row, with their absolute uncertainties given in parentheses. The primary contributors to these uncertainties are listed at the top of the table, given in relative %.

Primary sources of uncertainty			
	$K_{\alpha 1}$ x ray	207.8 keV	531.5 keV
Counting statistics	0.5%	0.7%	0.4%
Self-attenuation in foils	1.1%	0.04%	0.01%
HPGe detector efficiency	2.1%	2.1%	1.8%
$P_{K_{\alpha 1}}$ x ray	2.1%		
Measured absolute BR for ^{167}Tm per 100 EC decays			
		41.9(16)	1.73(7)

As noted in Refs. [10,14], the branching ratio of the 207.8-keV transition can also be calculated by decay-scheme normalization, if it is assumed that the second-forbidden EC transition to the ground state is negligible. In this case, after correcting for the internal-conversion contribution to each observed γ ray, the sum of the intensities of all the transitions to the ground state must equal 100%. This calculation produces a branching ratio of 0.416(7) [10], which agrees well with our experimental determination of the branching ratio.

III. NEUTRON-ACTIVATION CROSS-SECTION MEASUREMENTS

A. Experiment

Quasimonoenergetic neutrons were produced by the ^{2}H$(d,n)^3$He reaction by bombarding a 3.0-cm-long deuterium gas cell [15] held at a pressure of 5.0 atm with deuterons

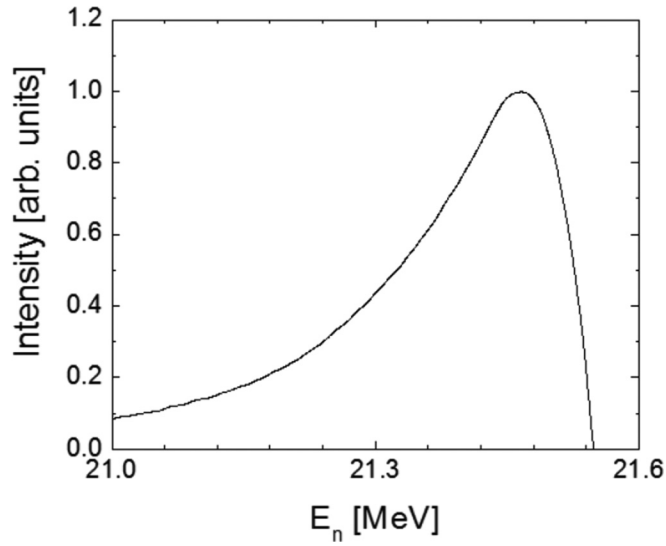

FIG. 5. Calculated energy distribution of neutrons striking the foil at the 21.5-MeV settings. The spread in neutron energies is primarily caused by kinematic effects from the extended geometry of the foil.

TABLE III. Deuteron energies (E_D) for the five experimental runs at TUNL and the corresponding neutron energies (E_n). The E_n on axis and the average value of E_n are listed. The energy spread of the neutrons striking the foils is from primarily the energy spread of the reacting deuterons and the angular dependence of the neutron energy distribution in the ^{2}H(d,n)^{3}He reaction.

E_D (MeV)	On axis E_n (MeV)[a]	Average E_n (MeV)[b]	Energy spread FWHM (MeV)
15.02	17.5	17.35	0.18
16.06	18.5	18.34	0.18
17.12	19.5	19.33	0.19
18.12	20.5	20.32	0.19
19.22	21.5	21.31	0.20

[a]Neutron energy calculated for reactions at the center of the gas cell based on the magnet settings.
[b]Average energy of neutrons striking the activation foils.

accelerated by the High-Voltage FN Tandem Van de Graaff accelerator at TUNL. A stack of 0.9525-cm-diameter foil disks of ^{169}Tm, ^{nat}Ni, and ^{nat}Zr with properties listed in Table I was placed 0.9 cm from the end of the gas cell. Over five experimental runs, deuterons with energies E_D of 15.0–19.2 MeV were used to produce monoenergetic neutrons with energies of 17.5 to 21.5 MeV along the beam axis.

The energy distribution of these neutrons impinging on the foil is broadened by two effects. First, the reacting deuterons have an energy spread caused by energy-loss effects in the 6.5-μm Havar entrance foil and across the gas cell. These effects were determined by a Monte Carlo method using the Stopping Range in Matter (SRIM) program [16]. Second, with such a small distance between the gas cell and the activation foils, neutrons emitted off the beam axis can strike the foil. Because of the kinematics, the off-axis neutrons have a lower energy than the neutrons emitted parallel to the deuteron beam. This kinematic effect was taken into account using the differential cross section of the ^{2}H(d,n)^{3}He reaction [17] and assuming uniform production along the length of the gas cell. As an example, for 21.5-MeV neutrons produced at the center of the gas cell, the energy distribution of the neutrons hitting the foils is shown in Fig. 5. The spread in neutron energies at other settings is similar in shape. A summary of the average energies of the neutrons in the monoenergetic peak and their energy spread is presented in Table III.

Deuteron breakup contributes additional neutrons with lower energies from reactions in the deuterium gas cell, entrance collimator, Havar entrance foil, and tantalum beam stop. The neutron-energy distribution was determined at each energy setting so that the activation by lower-energy neutrons could be corrected. The neutron beam was pulsed and the neutron time of flight (NTOF) was measured with a 3.81-cm-diameter × 3.81-cm-long cylindrical liquid scintillation (BC501A) neutron detector placed along the beam axis at a distance of 287.5 cm from the end of the gas cell. The measured NTOF distributions [Fig. 6(a)] were converted to neutron energy spectra [Fig. 6(b)] using relativistic kinematics. The

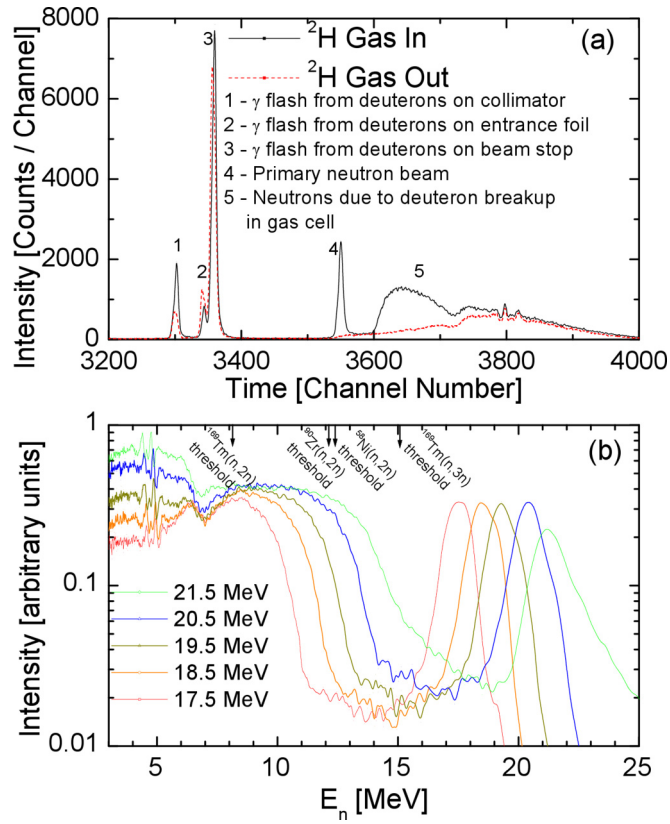

FIG. 6. (a) Time-of-flight spectrum for the settings used to produce 20.5-MeV neutrons. Additional measurements were performed with ^{2}H removed from the gas cell to help identify features noted in the plot. (b) Neutron-energy spectra determined from time-of-flight measurements. The spectra are normalized by area in the quasimonoenergetic peak and are shown with equal energy bin widths. The time-of-flight measurement at the 21.5-MeV settings was performed under timing conditions that resulted in greater broadening of the highest-energy neutrons.

TABLE IV. Flux correction (FC) factors calculated by Eq. (2) to account for activation by lower-energy neutrons produced from deuteron breakup.

Reaction energy (MeV)	^{90}Zr(n,2n)^{89}Zr FC	^{169}Tm(n,2n)^{168}Tm FC	^{169}Tm(n,3n)^{167}Tm FC	^{58}Ni(n,2n)^{57}Ni FC	^{94}Zr(n,α)^{91}Sr FC
17.35(10)	0.0523(26)	0.394(20)	0.00593(30)	0.0422(21)	0.118(6)
18.34(10)	0.0735(37)	0.609(30)	0.0108(5)	0.0590(3)	0.189(9)
19.33(10)	0.122(6)	0.765(38)	0.0224(11)	0.0950(5)	0.301(15)
20.32(10)	0.210(11)	0.856(21)	0.0424(21)	0.149(7)	0.438(22)
21.31(10)	0.440(22)	0.924(46)	0.117(6)	0.331(16)	0.645(32)

TABLE V. Decay data for nuclear reactions used in this work [23].

Reaction	Q value (MeV)	Product half-life	E_γ (keV)	I_γ
^{90}Zr$(n,2n)^{89}$Zr	−11.7	78.41(12) h	909.15(15)	0.9904(3)
^{169}Tm$(n,2n)^{168}$Tm	−8.03	93.1(2) d	198.251(2)	0.5449(16)
			815.989(5)	0.5095(16)
^{169}Tm$(n,3n)^{167}$Tm	−14.9	9.25(2) d	207.801(5)	0.419(16)
^{58}Ni$(n,2n)^{57}$Ni	−12.2	35.60(6) h	1377.63(3)	0.817(24)
^{94}Zr$(n,\alpha)^{91}$Sr	+2.03	9.63(5) h	1024.3(1)	0.335(11)

finite time resolution of the pulsing system, as determined by the width of the γ-ray flash from deuterons on the collimator, dominates the observed width of the quasimonoenergetic peak. The energy of the quasimonoenergetic neutron peaks measured in this way were consistent with the estimates based on the Tandem settings. The neutron detection threshold was determined using ^{22}Na, ^{88}Y, and ^{241}Am-Be sources and the resulting neutron detection efficiency was calculated with the NEFF7 code [18] as described in Ref. [19]. Only the relative neutron efficiency was required for the corrections applied.

At these deuteron energies, the breakup is significant, as can be seen in Fig. 6. To correct for activation from lower-energy neutrons, Eq. (2) was used to determine the fractional contribution (FC) of the activity induced from the breakup neutrons relative to the total activity induced [20],

$$\mathrm{FC} = \frac{\int_0^{E_c} \phi(E)\sigma(E)dE}{\int_0^{E_c} \phi(E)\sigma(E)dE + \phi_x\sigma_x}. \quad (2)$$

In Eq. (2), $\phi(E)$ is the neutron energy distribution determined by the NTOF measurements, $\sigma(E)$ is the cross section for the reaction of interest, E_c is the cutoff energy taken as the minimum point in the valley between the neutron peak and the deuteron breakup, ϕ_x is the integration of the neutron peak, and σ_x is the cross section at the peak energy. This factor was determined for each reaction of interest using excitation functions from nuclear data evaluations.

In all cases, only the shape of the cross section impacted the correction. The calculated FC values were more sensitive to uncertainties in the neutron-energy distribution than to differences between evaluated cross sections. For Tm(n,Xn) reactions, the ENDF/B-VII.1 evaluation was used. For the reactions that do not have ENDF evaluations above 20 MeV, other sources were used. Data for the ^{90}Zr$(n,2n)$ reaction were taken from the International Nuclear Data Committee evaluation [21], while for the ^{94}Zr(n,α) reaction, the JEFF-3.2 evaluation [22] was used and for the ^{58}Ni$(n,2n)$ reaction, the IRDFF-1.05 evaluation [22] was used. Uncertainty in FC includes the uncertainty from the excitation curve and the measured NTOF distribution propagated through Eq. (2). The calculated flux corrections for each energy and isotope are shown in Table IV.

The activation foils were counted on coaxial HPGe detectors at TUNL immediately following neutron irradiation. The foils were subsequently shipped to UC Berkeley for further counting. The primary γ-ray lines used for identifying isotopes are listed in Table V. Corrections were made for the minor variations in beam current during activation [24] and the decay of the sample between production and measurement using the half-lives in Table V. The uncertainties in these decay corrections are less than 1% because all the half-lives are precisely known. The neutron attenuation through the foils was calculated to be negligible, however, self-attenuation of the emitted γ rays in the foils was determined and used for subsequent corrections. All detectors were calibrated using standard sources. In both locations, samples were counted at a distance of 10 cm. Summing effects were determined using a GEANT4 simulation [25] of the detector and its surroundings. The corrections required were minimal, and the most significant were ∼2%.

B. Results

The neutron flux was determined from the ^{90}Zr$(n,2n)^{89}$Zr monitor reaction using the cross section from Ref. [21], which had uncertainties which varied between 1.44% to 3.46% in the energy range studied.

Cross sections were measured for the reactions listed in Table VI. For the ^{169}Tm$(n,2n)$ and ^{94}Zr(n,α) reactions, for which the monoenergetic neutron peak was much higher in energy than the reaction threshold, the flux correction (Table IV) was the largest contributor to uncertainty. The agreement of the present ^{169}Tm$(n,2n)$ cross-section results with previous experimental data [26] demonstrates that the

TABLE VI. Measured cross sections.

Reaction energy (MeV)	^{169}Tm$(n,2n)^{168}$Tm σ (b)	^{169}Tm$(n,3n)^{167}$Tm σ (b)	^{58}Ni$(n,2n)^{57}$Ni σ (b)	^{94}Zr$(n,\alpha)^{91}$Sr σ (b)
17.35(10)	1.75(12)	0.279(15)	0.056(4)	0.0078(12)
18.34(10)	1.44(14)	0.593(31)	0.062(4)	0.0083(12)
19.33(10)	1.05(19)	0.861(54)	0.065(5)	0.0074(11)
20.32(10)	0.804(134)	1.06(7)	0.069(5)	0.0077(12)
21.31(10)	0.611(369)	1.27(10)	0.072(5)	0.0065(13)

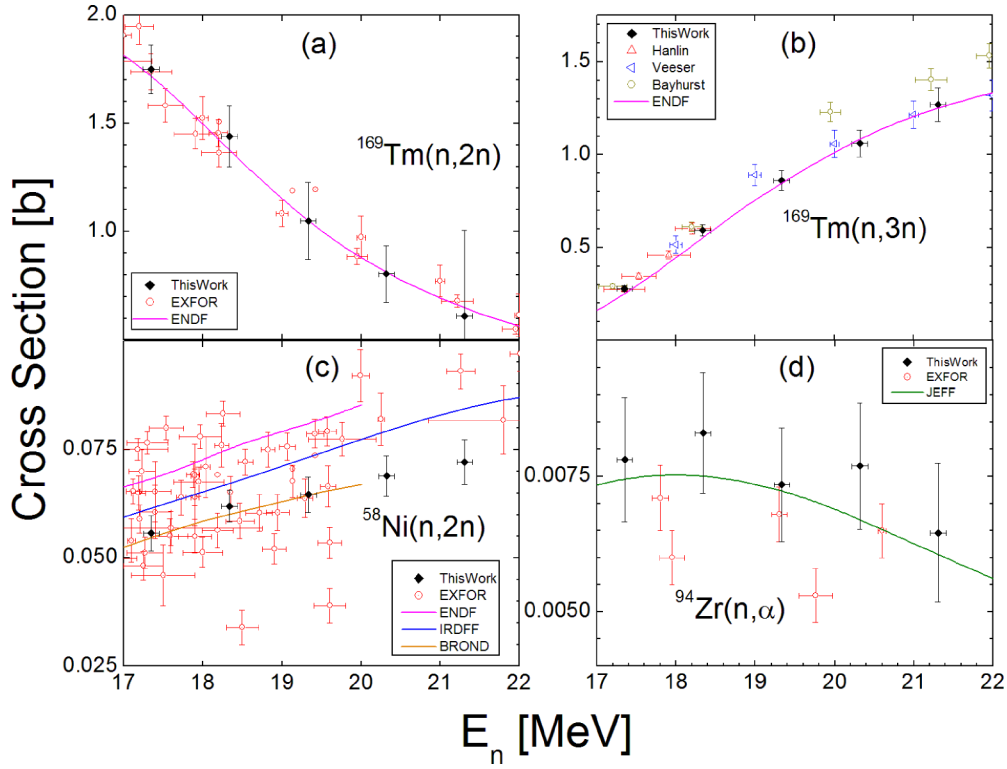

FIG. 7. Experimental results from this work compared with the previous data summarized in EXFOR and evaluations [22,26].

NTOF measurements and lower-energy-neutron correction techniques are reliable. This provides confidence in the smaller corrections applied for other reactions. Other significant sources of uncertainty were HPGe γ-ray detection efficiency (2%–3%), and in some cases, the γ-ray branching ratios. Other factors in the calculation contribute uncertainties of less than 1%.

The detection of the 207.8-keV γ ray simplifies the measurement of ^{167}Tm production and minimizes the assumptions required to interpret the data. The results for ^{169}Tm$(n,3n)^{167}$Tm, support the ENDF evaluation and are in agreement with the data of Veeser *et al.* [5] as can be seen in Fig. 7(b). These ^{169}Tm$(n,3n)$ cross-section results are about 15%–20% lower than those from Ref. [6] at energies around 20 MeV.

Existing experimental cross-section data for the ^{58}Ni$(n,2n)^{57}$Ni reaction is discrepant [26]. As shown in Fig. 7(c), the uncertainty of the individual measurements is of the order of 10%, however, the literature values for this cross section span nearly a factor of two in the energy range 17–22 MeV. The present data agree with the evaluation by Brond [22].

Results for ^{94}Zr$(n,\alpha)^{91}$Sr are also reported for which only two other measurements have been made in this energy region [27,28]. Although the (n,α) cross section is much smaller than the $(n,2n)$ and $(n,3n)$ cross sections for ^{94}Zr, it carries important additional information that constrains nuclear models used to determine optical model and energy level density parameters. Our ^{94}Zr(n,α) cross-section results support the JEFF-3.2 evaluation.

IV. SUMMARY

The motivation for this work was to solidify the nuclear data used to interpret an activation diagnostic that measures the yield of reaction-in-flight neutrons at NIF. The ^{169}Tm$(n,3n)^{167}$Tm reaction cross section and the branching ratio of the 207.8-keV γ ray following the EC decay of ^{167}Tm were remeasured.

The branching ratio was measured using the facilities at UC Berkeley and the 88-Inch Cyclotron at LBNL. A thin holmium foil was irradiated using a 29-MeV α-particle beam inducing the ^{165}Ho$(\alpha,2n)^{167}$Tm reaction. The foil was counted using well-calibrated coaxial and planar HPGe detectors. The branching ratios for the emission of 207.8-keV and 531.5-keV γ rays were determined with fractional uncertainties of approximately 3.8%. These uncertainties are five times smaller than the previous measured results [23].

Using this measured branching ratio for the 207.8-keV transition, a subsequent experiment was conducted to measure the ^{169}Tm$(n,3n)^{167}$Tm cross section. Quasimonoenergetic neutron beams were produced using the 10-MV Van de Graaff accelerator at TUNL. The cross section was measured with a precision of 5%–8% in the 17–22 MeV energy range that is important for determining the RIF-neutron fluence at NIF. In addition, the cross sections for ^{58}Ni$(n,2n)$ and ^{94}Zr(n,α) were measured over the same energy range.

These branching-ratio and cross-section results provide reliable nuclear data which reduce the overall uncertainties on the measured reaction-in-flight yield at NIF to about 5%–8% in an important energy region between 17 and 22 MeV. This

work confirms the ^{169}Tm$(n,3n)^{167}$Tm cross section ENDF evaluation and the Veeser *et al.* [5] results and provides strong evidence that the experimental results of Bayhurst *et al.* [6] are 15%–20% too large.

ACKNOWLEDGMENTS

We thank the operations and staff at Lawrence Berkeley National Laboratory 88-Inch Cyclotron and the Triangle Universities Nuclear Laboratory Accelerator facilities for their support in performing these experiments. We thank E. Browne and C. Baglin for discussions regarding the Table of Isotopes and Nuclear Data Sheets data, M. Bhike for activation assistance at TUNL, and C. Cerjan for valuable discussions regarding RIF neutron production. This work was performed under the auspices of the US Department of Energy by Lawrence Berkeley National Laboratory under Contract No. DE-AC02-05CH11231, Lawrence Livermore National Laboratory under Contract No. DE-AC52-07NA27344, with funding support from the Laboratory Directed Research and Development Program under project 15-ERD-015, and the University of California under Contract No. DE-AC0376SF0098. We also thank the US Department of Energy's NNSA, Office of Nonproliferation Research and Development (NA-22), for financial support. This material is based upon work supported by the Department of Energy National Nuclear Security Administration under Grant No. DE-NA-0000979 through the Nuclear Science and Security Consortium. Finally, this work was supported by the US Department of Energy, Grant No. DE-FG-97ER40133, and by the National Nuclear Security Administration under Grant No. DA-NA-0001839, both to Duke University.

[1] P. A. Bradley, G. P. Grim, A. C. Hayes, G. Jungman, R. S. Rundberg, J. B. Wilhelmy, and G. M. Hale, Neutron reactions in the hohlraum at the LLNL National Ignition Facility, Phys. Rev. C **86**, 014617 (2012).

[2] O. A. Hurricane, D. E. Hinkel, D. A. Callahan, D. T. Casey, P. M. Celliers, C. Cerjan, E. L. Dewald, T. R. Dittrich, T. Do, L. F. B. Hopkins, J. L. Kline, S. L. Pape, A. G. Macphee, J. L. Milovich, A. Pak, and P. K. Patel, Fuel gain exceeding unity in an inertially confined fusion implosion, Nature (London) **506**, 343 (2014).

[3] A. C. Hayes, G. Jungman, A. E. Schulz, M. Boswell, M. M. Fowler, G. Grim, A. Klein, R. S. Rundberg, J. B. Wilhelmy, D. Wilson, C. Cerjan, D. Schneider, S. M. Sepke, A. Tonchev, and C. Yeamans, Reaction-in-flight neutrons as a test of stopping power in degenerate plasmas, Phys. Plasmas **22**, 082703 (2015).

[4] L. Han-Lin, Z. W. Rong, and F. P. Guo, Measurement of the neutron cross sections for the reactions Tm$(n,3n)$ 167 Tm, Nucl. Sci. and Eng. **90**, 304 (1985).

[5] L. R. Veeser, E. D. Arthur, and P. G. Young, Cross sections for $(n,2n)$ and $(n,3n)$ reactions above 14 MeV, Phys. Rev. C **16**, 1792 (1977).

[6] B. P. Bayhurst, J. S. Gilmore, R. J. Prestwood, J. B. Wilhelmy, N. Jarmie, B. H. Erkkila, and R. A. Hardekopf, Cross sections for (n, xn) reactions between 7.5 and 28 MeV, Phys. Rev. C **12**, 451 (1975).

[7] L. Funke and W. Andrejtscheff, Niveaustruktur in ^{167}Er, Nucl. Phys. A **118**, 97 (1968).

[8] M. J. Berger, J. H. Hubbell, S. M. Seltzer, J. Chang, J. S. Coursey, R. Sukumar, D. S. Zucker, and K. Olsen, *XCOM Photon Cross Section Database (Version 1.5)* (National Institute of Standards and Technology, Gaithersburg, MD, 2010), Online Available: http://physics.nist.gov/xcom.

[9] M. Gooden, Energy dependence of fission product yields from 235U, 238U, and 239Pu for incident neutron energies between 0.5 and 14.8 MeV, Ph.D thesis, North Carolina State University, 2014.

[10] C. M. Baglin, Nuclear data sheets for $A = 167$*, Nucl. Data Sheets **90**, 431 (2000).

[11] E. Schönfeld, Calculation of fractional electron capture probabilities, Appl. Radiat. Isot. **49**, 1353 (1998).

[12] T. Kibédi, T. W. Burrows, M. B. Trzhaskovskaya, P. M. Davidson, and C. W. Nestor, Evaluation of theoretical conversion coefficients using BrIcc, Nucl. Inst. and Meth A **589**, 202 (2008).

[13] R. Firestone, *Table of Isotopes*, 8th ed. (Wiley & Sons, New York, 1996).

[14] E. Browne, Branching ratios derived from decay schemes, Nucl. Instr. and Meth. A **249**, 461 (1986).

[15] C. Bhatia, B. Fallin, M. E. Gooden, C. R. Howell, J. H. Kelley, W. Tornow, C. W. Arnold, E. M. Bond, T. Bredeweg, M. M. Fowler, W. Moody, R. S. Rundberg, G. Rusev, D. J. Vieira, J. B. Wilhelmy, J. Becker, R. Macri, C. Ryan, S. Sheets, M. Stoyer, and A. P. Tonchev, Dual-fission chamber and neutron beam characterization for fission product yield measurements using monoenergetic neutrons, Nucl. Inst. and Meth. A **757**, 7 (2014).

[16] J. F. Ziegler, M. D. Ziegler, and J. P. Biersack, SRIM—The stopping and range of ions in matter (2010), Nucl. Instr. and Meth. B **268**, 1818 (2010).

[17] M. Drosg, Unified absolute differential cross sections for neutron production by the hydrogen isotopes for charged particle energies between 6 and 17 MeV, Nucl. Sci. Eng. **67**, 190 (1978).

[18] G. Dietze and H. Klein, *NRESP4 and NEFF4- Monte Carlo Codes for the Calculation of Neutron Response Functions and Detection Efficiencies for NE 213 Scintillation Detectors, PTB-ND-22* (Physikalisch Technische Bundesanstalt, 1982).

[19] B. Nilsson, High-resolution measurement of the He(γ,n) reaction in the giant resonance region, Ph.D. thesis, Lund University, 2003.

[20] K. Kawade, H. Sakane, Y. Kasugai, M. Shibata, T. Iida, A. Takahashi, and T. Fukahori, Measurement method of activation cross sections of reactions producing short-lived nuclei with 14 MeV neutrons, Nucl. Inst. and Meth. A **496**, 183 (2003).

[21] K. I. Zolotarev, Re-evaluation of Cross-Section Data from Threshold to 40–60 MeV for Specific Nuclear Reactions Important for Neutron Dosimetry Applications, INDC(NDS)-0546 (International Atomic Energy Agency, Vienna, Austria, 2009).

[22] Evaluated Nuclear Data File, http://www.nndc.bnl.gov/exfor/endf11.jsp.

[23] Interactive Chart of Nuclides, http://www.nndc.bnl.gov/chart/.

[24] A. P. Tonchev, C. T. Angell, M. Boswell, A. S. Crowell, B. Fallin, S. Hammond, C. R. Howell, A. Hutcheson, H. J. Karwowski, J. H. Kelley, R. S. Pedroni, W. Tornow, J. A. Becker, D. Dashdorj,

J. Kenneally, R. A. MacRi, M. A. Stoyer, C. Y. Wu, E. Bond, M. B. Chadwick, J. Fitzpatrick, T. Kawano, R. S. Rundberg, A. Slemmons, D. J. Vieira, and J. B. Wilhelmy, Measurement of the ^{241}Am$(n,2n)$ reaction cross section from 7.6 to 14.5 MeV, Phys. Rev. C **77**, 054610 (2008).

[25] S. Agostinelli, J. Allison, K. Amako, J. Apostolakis, and H. Araujo, GEANT4—a simulation toolkit, Nucl. Inst. and Meth. A **506**, 250 (2003).

[26] Experimental Nuclear Reaction Data (EXFOR), http://www.nndc.bnl.gov/exfor/exfor.htm.

[27] V. Semkova, E. Bauge, A. J. M. Plompen, and D. L. Smith, Neutron activation cross sections for zirconium isotopes, Nucl. Phys. A **832**, 149 (2010).

[28] B. P. Bayhurst and R. J. Prestwood, (n, p) and (n, a) excitation functions of several nuclei from 7.0 to 19.8 MeV, J. Inorg. Nucl. Chem. **23**, 173 (1961).